Showcasing research from Prof. Per-Anders Carlsson's group at Chalmers University of Technology, Gothenburg, Sweden.

Desorption products during linear heating of copper zeolites with pre-adsorbed methanol

Catalysis has shaped our past and will shape our future. We explore new catalytic materials, their molecular function and ways to use them for environmental protection and chemical production without risking sustainability. We make materials and study their properties with time-resolved spectroscopic and scattering methods in controlled environments and most often while monitoring their efficiency. This work investigates the desorption products from pre-adsorbed methanol on MFI and CHA zeolites with or without copper upon heating with relevance for many hydrocarbon conversion reactions.

As featured in:

ROYAL SOCIETY
OF **CHEMISTRY**

rsc.li/pccp

PAPER

Check for updates

Desorption products during linear heating of copper zeolites with pre-adsorbed methanol†

Xueting Wang, [ab] Adam A. Arvidsson, [bc] Magnus Skoglundh, [ab] Anders Hellman[bc] and Per-Anders Carlsson *[ab]

Desorption products from zeolites with medium (MFI) and small (CHA) pores and with and without ion-exchanged copper were studied during linear heating after the pre-adsorption of methanol using a chemical flow reactor with a gas phase Fourier transform infrared spectrometer. The methanol desorption profiles were deconvoluted and compared with those predicted from first-principles calculations. *In situ* diffuse reflectance infrared Fourier transform spectroscopy was used to study the samples during methanol desorption following a step-wise increase of the sample temperature. It is shown that well-dispersed copper species in the Cu-zeolite samples interact more strongly with methanol and its derivatives as compared to the bare zeolites, resulting in methanol desorption at higher temperatures. Moreover, the introduction of Cu leads to CO formation and desorption in larger amounts at lower temperatures compared to the bare zeolites. The formation and desorption of dimethyl ether (DME) from pre-adsorbed methanol takes place at different temperatures depending on both the influence of Cu and the zeolite topology. The Cu sites in zeolites lead to higher DME formation/desorption temperatures, while a small shift of DME desorption towards higher temperatures is observed for the CHA framework structure compared to the MFI framework structure.

1 Introduction

Zeolites have been used as catalysts in many applications due to their microporosity and surface acidity that can be utilised for controlling the product selectivity in acid catalysed reactions. Over the years, their hydrothermal stability has been improved and the pores and cages can accommodate various elements that function as active species, such as copper ions, in reactions.[1–3] Despite their high framework crystallinity, mechanistic studies and modelling studies are challenging due to their complex framework structures and rich variety of their chemical composition and defect density. The protonic form of zeolites is active for many acid catalysed reactions such as methanol to hydrocarbons or olefins, where the Brønsted acid

sites play important roles.[4–6] Upon ion-exchange with copper, various Cu species, such as monomers, dimers and small clusters, are formed depending on the parent zeolite composition/structure and the ion-exchange level.[7–9] The redox properties of these Cu species can help in the catalysis of selective oxidation reactions such as methane to methanol or acetic acid.[10–12] When the Cu/Al ratio is below 0.5, both Brønsted acid sites and Cu sites are present in the Cu-zeolite, which may facilitate the interplay of these sites and contribute to more complex mechanisms for reactions such as NO_x reduction[13] and methane to methanol.[14] Commonly, probe molecules such as NH_3 combined with temperature-programmed desorption (TPD) are used for the identification of acid sites in zeolites,[15,16] whereas molecules such as H_2, N_2, CO or suitable hydrocarbons are used to probe Cu sites in Cu-zeolites.[17–19]

In this study we use methanol-TPD as a valuable method for the investigation of the dynamic interaction between methanol and zeolite materials.[20–22] This can bring valuable insights into reactions such as methanol-to-hydrocarbons, where the selectivity for different products depends largely on the framework structure and acidity of the zeolites.[2,6] Methanol is adsorbed and converted to surface methoxy species on the Brønsted acid sites, which initiate further reactions towards hydrocarbons.[23–25] In this respect, the characterization of zeolites using methanol as a probe molecule can reveal the impact of topology and acidity on important elementary steps and chemical reactions.

a Department of Chemistry and Chemical Engineering, Chalmers University of Technology, 412 96 Gothenburg, Sweden. E-mail: per-anders.carlsson@chalmers.se
b Competence Centre for Catalysis, Chalmers University of Technology, 412 96 Gothenburg, Sweden
c Department of Physics, Chalmers University of Technology, 412 96 Gothenburg, Sweden

† Electronic supplementary information (ESI) available: Calculation of the amount of adsorption sites; desorption profile of main gas phase species; DME desorption and NH_3 desorption profiles of the Cu-ZSM-5, H-ZSM-5, Cu-SSZ-13, H-SSZ-13, Cu/SiO$_2$ and SiO$_2$ samples; IR spectra recorded during methanol desorption; a table of binding energies and desorption peak maxima for all calculated adsorption sites; sensitivity analysis on the calculated desorption spectra. See DOI: 10.1039/c9cp05479k

This journal is © the Owner Societies 2020

Phys. Chem. Chem. Phys., 2020, **22**, 6809–6817 | **6809**

Zeolites with medium and small pore sizes, such as ZSM-5 with MFI and SSZ-13 with CHA framework structures, are commonly used as catalysts. The MFI framework structure includes channels whereas the CHA framework consists of cages.[26] The shape and pore dimensions steer the product selectivity in the methanol-to-hydrocarbon process[2,6,27] and can possibly host different copper species active for the conversion of methane to methanol.[3,11,28,29] In this study, we focus on two Cu-zeolite samples with the MFI or CHA framework structure (Cu-ZSM-5 and Cu-SSZ-13), respectively. The typical Cu species present in Cu-ZSM-5 and Cu-SSZ-13 samples have been studied in the previous literature[7,29–33] and can give guidance on the Cu speciation of our samples. According to these studies the Cu-ZSM-5 sample with a medium Cu/Al ratio (0.38) and a relatively low Si/Al ratio (13.5) should contain a large proportion of Cu-oxo species such as dimers and trimers.[7,30,31] However, for the Cu-SSZ-13 sample with both low Cu/Al (0.13) and Si/Al (10) ratios, Cu monomers located in the six-membered rings with two Al are common, while Cu dimers are not commonly observed.[29,31–33]

This study speciates the desorption products during linear heating of zeolites and Cu-zeolites (with MFI and CHA framework structures) after methanol exposure, with SiO_2 and Cu/SiO_2 as references. The methanol desorption profiles have been deconvoluted and compared with those predicted from first-principles calculations. *In situ* diffuse reflectance infrared Fourier transform spectroscopy (DRIFTS) has been used to study the surface species on the samples during methanol desorption following a step-wise increase of the temperature. It is shown that copper species in the zeolites interacts more strongly with methanol and its derivatives than the zeolitic Brønsted acid sites. Moreover, the formation and desorption of DME from pre-adsorbed methanol occur at higher temperatures for the samples with Cu modification. Furthermore, the zeolite topology has a minor influence on the DME desorption temperature, which is slightly higher for the CHA framework structure than for the MFI framework structure.

2 Methods

2.1 Sample preparation

The preparation of the Cu-ZSM-5, Cu-SSZ-13 and Cu/SiO_2 samples has been described in detail previously.[22,34] Briefly, the Cu-ZSM-5 and Cu-SSZ-13 samples were prepared using aqueous ion-exchange in which each parent zeolite (H-ZSM-5, Si/Al = 13.5; or H-SSZ-13, Si/Al = 10) was mixed with an aqueous solution of $Cu(NO_3)_2$ (Sigma-Aldrich, ACS reagent, 0.1 M, 100 ml g^{-1} zeolite) for 24 h. The suspension was filtered and dried at 120 °C overnight to give the powder sample. The Cu/SiO_2 sample was prepared using incipient wetness impregnation where an aqueous solution of $Cu(NO_3)_2 \cdot 5H_2O$ (Sigma-Aldrich, ACS reagent, 0.29 M, 1.66 ml g^{-1} silica) was slowly added to the silica (Akzo Nobel, Kromasil, 200 Å, 5 μm). The mixture was then freeze-dried over night and calcined in air at 350 °C for 3 h.

The basic characteristics of the powder samples have been reported in our previous study.[34] Shortly, the X-ray diffraction

(XRD) results show that the zeolite framework structures of the Cu-zeolite samples are well-preserved during the Cu ion-exchange process. The Cu species in the Cu-ZSM-5 and Cu-SSZ-13 samples are mainly isolated Cu ions and clusters according to *ex situ* X-ray absorption spectroscopy analysis, whereas the Cu/SiO_2 sample (predominantly) consists of CuO nanoparticles with an average size of 28.3 nm as calculated from the XRD pattern. The copper loading measured with an inductively coupled plasma-sector field mass spectrometer (ICP-SFMS) is 2.8 and 1.3 wt% for the Cu-ZSM-5 and Cu-SSZ-13 samples, respectively. The calculated Cu/Al ratio is 0.38 and 0.13 for the Cu-ZSM-5 and Cu-SSZ-13, respectively. The Cu loading for the Cu/silica sample was calculated to be 3.0 wt%.

Monolith samples for the flow reactor study were prepared by wash-coating each powder sample on cordierite monolith substrates (Corning, 400 cpsi, L = 15 mm, and Ø = 13 mm). The wash-coating procedure is described elsewhere.[34] Approximately 0.16 g of each powder sample was coated on the monoliths using water dispersible boehmites (Sasol, Disperal P2) as the binder.

2.2 Desorption experiments

2.2.1 Flow reactor measurements. The desorption profiles were recorded using a flow reactor system with a controlled evaporation mixer system (Bronkhorst Hi-tech) for methanol feeding and a Fourier transform infrared spectrometer (MKS 2030 FTIR spectrometer) for effluent gas analysis. The flow reactor system is described in detail elsewhere.[35] Six monolith samples were investigated, *i.e.* H-ZSM-5, H-SSZ-13, SiO_2, Cu-ZSM-5, Cu-SSZ-13 and Cu/SiO_2. All samples were pre-treated under either oxidizing (10 vol% O_2) or reducing (1.5 vol% H_2) environments at 500 °C for 30 min. For the methanol desorption measurements, the samples were cooled to 80 °C in pure Ar and fed with 600 ppm methanol (99.8%, Acros Organics) for 1 h at 80 °C. After methanol exposure, the samples were kept in Ar at 80 °C for 50 min. The total flow was kept constant at 1500 ml min^{-1} (GHSV = 34 000 h^{-1}) with Ar as the balancing gas during the pre-treatment and methanol exposure. Subsequently, the samples were stabilized under a 500 ml min^{-1} Ar flow (GHSV = 11 300 h^{-1}) at 80 °C (10 min). The desorption part of the experiment was then carried out under a 500 ml min^{-1} flow of Ar with a temperature ramp of 5 °C min^{-1}.

2.2.2 *In situ* infrared spectroscopy measurements. Infrared spectroscopy (IR) measurements during methanol desorption were carried out in a diffuse reflectance mode using a Vertex70 FTIR spectrometer (Bruker). The spectrometer is equipped with a liquid nitrogen cooled mercury cadmium telluride detector with a bandwidth of 600–12 000 cm^{-1}, a Praying Mantis™ diffuse reflectance accessory and a high-temperature stainless steel reaction chamber (Harrick Scientific Products Inc.). The spectra were recorded between 900 and 4000 cm^{-1} and the spectral resolution is 1 cm^{-1}. The instrumental aperture was 4 mm wide during measurements. A sieved fraction between 38 and 75 μm of the samples was used and about 85 μl of the sample was loaded in the sample cup.

Methanol desorption experiments were carried out for the Cu-ZSM-5, H-ZSM-5, Cu-SSZ-13, H-SSZ-13, Cu/SiO_2 and SiO_2

6810 | *Phys. Chem. Chem. Phys.*, 2020, **22**, 6809–6817

This journal is © the Owner Societies 2020

samples. After pre-treatment of the samples with O_2 at 550 °C for one hour, a few droplets of methanol (99.8%, Sigma-Aldrich) were added to the samples at 30 °C. The following desorption experiments were carried out under a 100 ml min^{-1} flow of pure Ar with a stepwise temperature increase from 30 °C to 450 °C. The backgrounds were recorded in pure Ar at 30 °C before methanol adsorption.

2.3 Theoretical methods

Theoretical calculations were performed with the Vienna ab initio simulation package (VASP) software[36,37] using the spin-polarized version of the Perdew–Burke–Ernzerhof (PBE)[38] exchange–correlation functional together with D3 van der Waals correction.[39] Only the Γ-point was used to sample the Brillouin zone. The energy cutoff was 400 eV and Gaussian smearing with a value of 0.05 eV was used. The convergence criterion between two subsequent steps in the self-consistent loop was 10^{-8} eV.

The geometry relaxation was considered to be converged when the maximum force was less than 0.03 eV Å^{-1}. Vibrational frequencies were calculated within the harmonic limit, using central differences to obtain the Hessian matrix with a displacement of 0.01 Å. Structural relaxations and vibrational frequencies were calculated using the Atomic Simulation Environment (ASE)[40] and VASP.

Cu monomer and dimer sites were modelled in the MFI (ZSM-5) and CHA (SSZ-13) frameworks (see Fig. S9 and S10, ESI†). In MFI, the Cu monomer sites were modelled over the Al T12 site[5] (Fig. S9a and b, ESI†), and the dimer was modelled over the $[Cu–O–Cu]^{2+}$ site[41,42] (Fig. S9d, ESI†). It is a known problem that semilocal exchange–correlation functionals delocalize the open spin states over the copper atoms in the system.[43] However, this only has a minor effect on methanol adsorption energies.[44] The silanol was modelled over the monomer silicon T-site from a dissociated water molecule (Figs. S9c and S10c, ESI†), forming two hydroxyl species with a calculated vibration frequency of around 3770 cm^{-1}, which agrees well with the experimental results.[22]

2.3.1 Calculated methanol desorption profiles. The theoretical methanol desorption profiles were calculated assuming an isolated, independent site where adsorption and desorption of methanol occur,[45,46] *i.e.* the process:

$$CH_3OH* \underset{k_d}{\overset{k_a}{\rightleftharpoons}} * + CH_3OH(g) \tag{1}$$
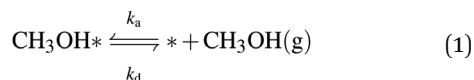
where $*$ denotes an adsorption site and $CH_3OH(g)$ is methanol in the gas phase. k_a and k_d are the rate constants for adsorption and desorption, respectively.

In the mean-field assumption, the change of coverage of methanol, θ, is

$$\frac{d\theta}{dt} = k_a \frac{p}{p_{ref}}(1 - \theta) - k_d\theta \tag{2}$$

where p is the partial pressure of methanol and p_{ref} is the reference pressure. Using the ideal gas law, the concentration of methanol can be expressed as in eqn. 3, assuming that

adsorption and desorption equilibrates quicker than the heating rate ($d\theta/dt \approx 0$),

$$C = \frac{N}{V} = \frac{p}{k_B T} = \frac{\theta}{1 - \theta}\frac{p_{ref}}{k_B T}\frac{k_d}{k_a} \tag{3}$$

where $K = k_d/k_a = \exp(-\Delta G/(k_B T))$ is the equilibrium constant. At the same time the mass balance in the flowing gas is

$$FC = -A_0 W\frac{d\theta}{dt} = -\beta A_0 W\frac{d\theta}{dT} \tag{4}$$

where F is the flow rate of the carrying gas, A_0 is the concentration of the adsorption sites, W is the sample weight and $\beta = dT/dt$ is the heating rate.

Using these two expressions for the concentration (3) and (4), the following relationship is obtained:

$$\frac{-\beta A_0 W}{F}\frac{d\theta}{dT} = \frac{\theta}{1 - \theta}\frac{p_{ref}}{k_B T}\exp\left(\frac{-\Delta G}{k_B T}\right) \tag{5}$$

where ΔG is calculated from first-principles calculations. Eqn (5) is solved iteratively using

$$\theta_{i+1} = \theta_i + \left(\frac{d\theta}{dT}\right)\Delta T \tag{6}$$

which, assuming a full initial coverage for each independent site, results in theoretical desorption profiles.

3 Results and discussion

The major gas phase products (methanol, DME and CO) formed during linear heating of all methanol exposed samples are shown in Fig. 1. In all cases, methanol desorbs mainly in the lower temperature range (below 250 °C), followed by DME formation at intermediate temperatures (130 to 350 °C), and CO formation solely at higher temperatures (above 250 °C). As shown in Fig. 1a, the desorption experiment for the Cu-ZSM-5 and Cu-SSZ-13 samples results in a larger amount of released methanol and also a broader desorption profile as compared to the parent H-ZSM-5 and H-SSZ-13 samples, respectively. Both observations indicate that the Cu ions/clusters in the Cu-ZSM-5 and Cu-SSZ-13 samples interact more strongly with methanol as compared to the sites in the parent zeolites. The desorption profiles for the Cu/SiO$_2$ and SiO$_2$ samples, however, exhibit considerably lower intensity with a desorption maximum at around 130 °C. The methanol desorbed from the SiO$_2$ sample is presumably attributed to the methanol pre-adsorbed on the silanol groups.[47] The slightly lower intensity and broader shape of the methanol desorption profile of the Cu/SiO$_2$ sample compared to that of the SiO$_2$ sample are likely due to CuO nanoparticles in the Cu/SiO$_2$ sample covering silanol sites responsible for methanol adsorption and creating new adsorption sites on the CuO nanoparticles. The small difference, however, between the methanol desorption profile for the Cu/SiO$_2$ and SiO$_2$ samples indicates that the adsorption of methanol is only affected to a minor extent by the presence of CuO, which is in contrast with the Cu ions/clusters in the Cu-zeolite samples.

This journal is © the Owner Societies 2020

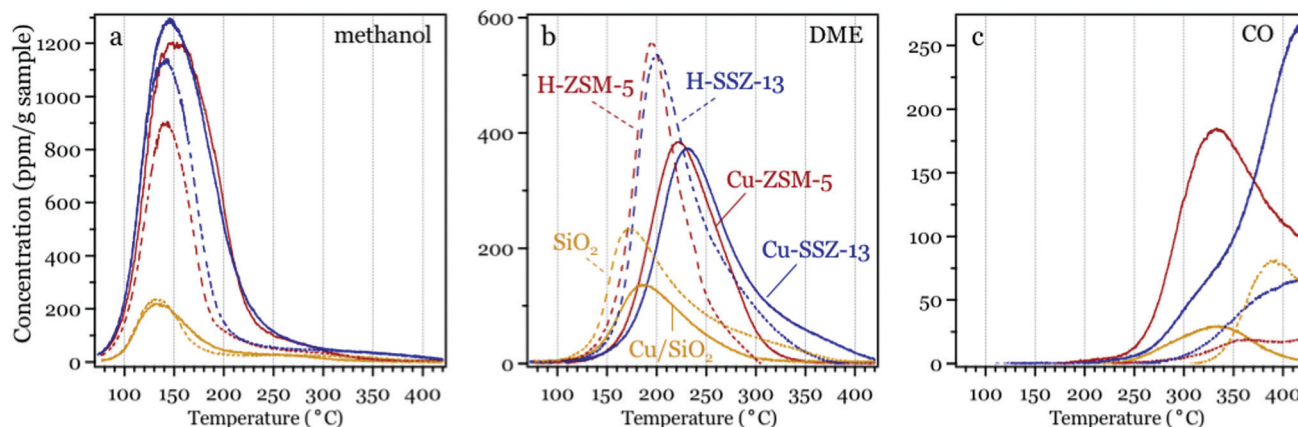*Phys. Chem. Chem. Phys.*, 2020, **22**, 6809–6817 | **6811**

Fig. 1 Desorption products during linear heating of oxidized Cu-ZSM-5 (red solid line), H-ZSM-5 (red dashed line), Cu-SSZ-13 (blue solid line), H-SSZ-13 (blue dashed line), Cu/SiO$_2$ (yellow solid line), and SiO$_2$ (yellow dashed line) samples with pre-adsorbed methanol. Panel (a) methanol, (b) DME and (c) CO.

During linear heating of the samples, DME is formed due to methanol dehydration over the acidic sites on the samples.[4,48] The DME desorption profiles of all samples are presented in Fig. 1b. It is evident that the Cu-exchanged zeolites release lower amounts of DME at temperatures lower than 220 °C and higher amounts of DME at temperatures exceeding 220 °C compared to the parent zeolites. The lower amount of DME desorption at lower temperatures for the Cu-ZSM-5 and Cu-SSZ-13 samples compared to the H-ZSM-5 and H-SSZ-13 samples might be due to the ion-exchange of Cu ions at the Brønsted acid sites and at framework defects in the Cu-ZSM-5 and Cu-SSZ-13 samples during the ion-exchange, resulting in blocking of acidic sites for low temperature DME formation. The DME desorption at higher temperatures (above 220 °C) for the Cu-zeolites is presumably a result from the stronger interaction between methoxy/DME and the Cu species in these samples compared to the zeolite samples. Moreover, DME desorbs at slightly lower temperatures from the samples with the MFI type of framework structure, i.e. the H-ZSM-5 and Cu-ZSM-5 samples, compared to the corresponding samples with the CHA type of framework structure, i.e. the H-SSZ-13 and Cu-SSZ-13 samples, respectively. This difference is presumably due to the different framework structures. It is anticipated that DME diffusion is faster in the MFI framework structure where the channels are easily accessed through 10-membered rings, while slower in the CHA framework structure where diffusion through 8-membered rings is limiting. Additionally, a considerable amount of DME forms from pre-adsorbed methanol at temperatures above 150 °C over the Cu-ZSM-5 and Cu-SSZ-13 samples, which suggests that low temperatures (<200 °C) are necessary for selectivity towards methanol when Cu-zeolites are used as catalysts for partial oxidation of methane to methanol. For the Cu/SiO$_2$ and SiO$_2$ samples, lower DME desorption with desorption maximum at lower temperatures is observed compared to all zeolite samples. The lower amount of DME formed over the Cu/SiO$_2$ sample compared to that of the SiO$_2$ sample is likely due to the CuO nanoparticles covering some silanol groups on the silica surface that are responsible for DME formation. Moreover, as the Cu/SiO$_2$ sample contains CuO nanoparticles dominantly while the Cu-zeolite samples consist of mostly Cu ions/clusters, the difference in DME desorption temperatures for the Cu/SiO$_2$ and the Cu-zeolite samples indicates that isolated Cu ions/clusters are responsible for the strong interaction with methanol and its derivative species rather than the CuO particles.

At temperatures higher than 250 °C, CO starts to desorb from the Cu containing samples while the CO desorption starts at a higher temperature (around 300 °C) for the zeolite and silica samples. The amount of CO desorbed from the Cu-zeolite samples is higher than that of the zeolite samples. The higher amount of CO formed over the Cu-zeolite samples is likely due to the ability of the Cu ions/clusters to oxidize the adsorbed methanol/methoxy species in the Cu-zeolite samples, which is in agreement with our previous study of methanol desorption using *in situ* IR spectroscopy.[22] Moreover, a large amount of CO desorbs at much lower temperatures for the Cu-ZSM-5 sample than the Cu-SSZ-13 sample with around 100 °C difference for the desorption maximum, while the amount of CO$_2$ formed and desorbed is much higher for the Cu-ZSM-5 sample compared to the Cu-SSZ-13 sample (Fig. S1b and S2b, ESI†). It is anticipated that such difference in the CO/CO$_2$ profile is a result of the difference in proportion of various Cu species in these two samples.

Interestingly, the oxidizing or reducing pre-treatment condition affects the desorption profile of the Cu containing samples (Fig. S1, S2, S3, ESI† panels a and b) but not the Cu free samples (Fig. S1, S2 and S3, ESI† panels c and d), which indicates that some Cu species, depending on the pre-treatment environment, are prone to changes. For both Cu-ZSM-5 and Cu-SSZ-13 samples, a higher amount of methanol, DME and formaldehyde are desorbed when the samples are pre-oxidized. The CO and CO$_2$ desorption profiles, however, are affected by pre-treatment conditions more significantly for the Cu-ZM-5 sample than the Cu-SSZ-13 sample. As discussed previously, the Cu-ZSM-5 sample should contain higher amounts of small Cu clusters such as dimers and trimers while the Cu-SSZ-13 sample contains Cu monomers dominantly. The difference in CO and CO$_2$ desorption profiles for the Cu-ZSM-5 could be due to the changes of these small Cu clusters which are insufficient in the Cu-SSZ-13 sample.
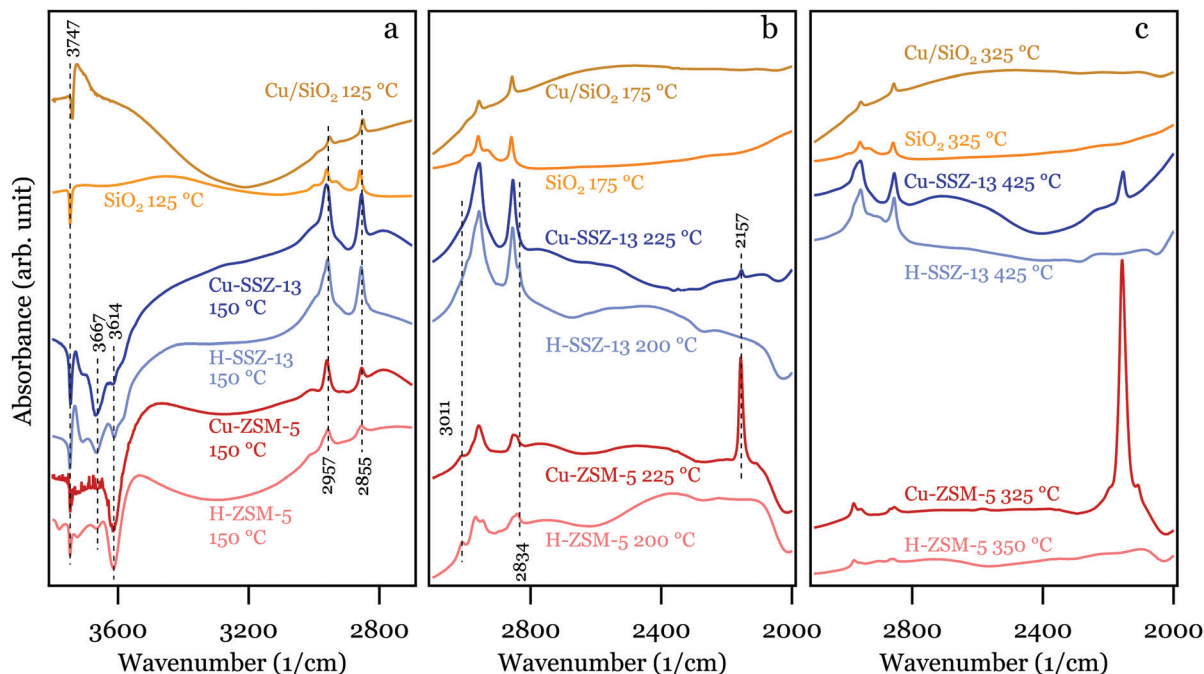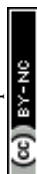
Fig. 2 IR spectra of selected wavenumber regions collected during methanol desorption at low temperatures (a), medium temperatures (b) and high temperatures (c) for the pre-oxidized Cu/SiO₂ (yellow), SiO₂ (light yellow), Cu-ZSM-5 (red), H-ZSM-5 (light red), Cu-SSZ-13 (blue) and H-SSZ-13 (light blue) sample.

The surface species formed during methanol desorption were followed by DRIFTS and selected regions of the spectra are presented in Fig. 2. The presented spectra were recorded at low temperatures (Fig. 2a) where the methanol desorption profile peaks and medium temperatures (Fig. 2b) where the DME desorption profile peaks and high temperatures (Fig. 2c) where CO desorption profile peaks for each sample (Fig. 1a–c), respectively. As shown in Fig. 2a, a double band at 2957 and 2855 cm^{-1}, originated from adsorbed methoxy groups,[22,49–51] is evident for all samples, indicating that methanol adsorbs and dissociates over all samples. Moreover, the negative bands at 3747, 3667 and 3614 cm^{-1} for the Cu-SSZ-13, H-SSZ-13, Cu-ZSM-5 and H-ZSM-5 samples are associated with the O–H stretching vibrations in isolated silanol, isolated hydroxyl on extra framework Al and Brønsted acid sites,[4,22,49–51] which are isolated vibrational structures disappearing due to their interaction with adsorbed methanol. For the Cu/SiO₂ and SiO₂ samples, however, only a negative band at 3747 cm^{-1} exists due to methanol interactions with isolated silanol groups. The lack of other negative bands coincides with the absence of Al in these two samples. At medium temperatures (Fig. 2b), absorption features originated from DME, *i.e.* the bands at 3011 and 2834 cm^{-1},[4] are visible for the zeolite and Cu-zeolite samples. The absorption bands associated with methoxy species, however, are prominent for all six samples. As minor amounts of methanol desorb for each sample in the medium temperature range (Fig. 1a), we speculate that the surface methoxy species on all six samples readily form DME in the medium temperature range that desorb into the gas phase. Moreover, the absorption bands associated with CO on Cu$^+$ (2157 cm^{-1})[52]

are evident for the Cu-ZSM-5 and Cu-SSZ-13 samples, suggesting that the methoxy species is further oxidized to CO on the Cu sites at medium temperatures. At high temperatures, as shown in Fig. 2c, absorption features in the C–H stretching vibration range of 2800–3000 cm^{-1} are evident but lower in intensity for all six samples. This indicates that surface methanol, methoxy and DME are desorbed to a large extent at such high temperatures. The remaining absorption features at this region, however, suggests that some methoxy species are strongly bonded to the surface and are probably the carbon source for CO formation. For the Cu-ZSM-5 and the Cu-SSZ-13 samples, Cu bonded CO is evident at high temperatures, suggesting that Cu species are responsible for the large amount of CO desorbed in Fig. 1c.

3.1 Deconvolution of the methanol desorption profiles

Deconvolution of the methanol profiles from the H-ZSM-5, Cu-ZSM-5, H-SSZ-13 and Cu-SSZ-13 samples is shown in Fig. 3. Four Gaussian functions are fitted to the methanol desorption profiles for both the H-ZSM-5 and H-SSZ-13 samples. For the Cu-ZSM-5 and Cu-SSZ-13 samples, three additional Gaussian functions (blue lines) are fitted to the methanol desorption profiles based on the four Gaussian functions from the H-ZSM-5 and H-SSZ-13 samples. For this, the three Gaussian functions centered at 133, 200 and 300 °C identical to the parent zeolites are used in the Cu-zeolites, respectively, while the Gaussian functions centered at 153 or 163 °C for the H-ZSM-5 or H-SSZ-13 sample are applied to the corresponding Cu-zeolite samples with reduced amplitude according to the ratio of Brønsted acid site concentrations in the Cu-zeolites and their parent zeolites, see the ESI,† Table S1. For the deconvolution, the least number

This journal is © the Owner Societies 2020

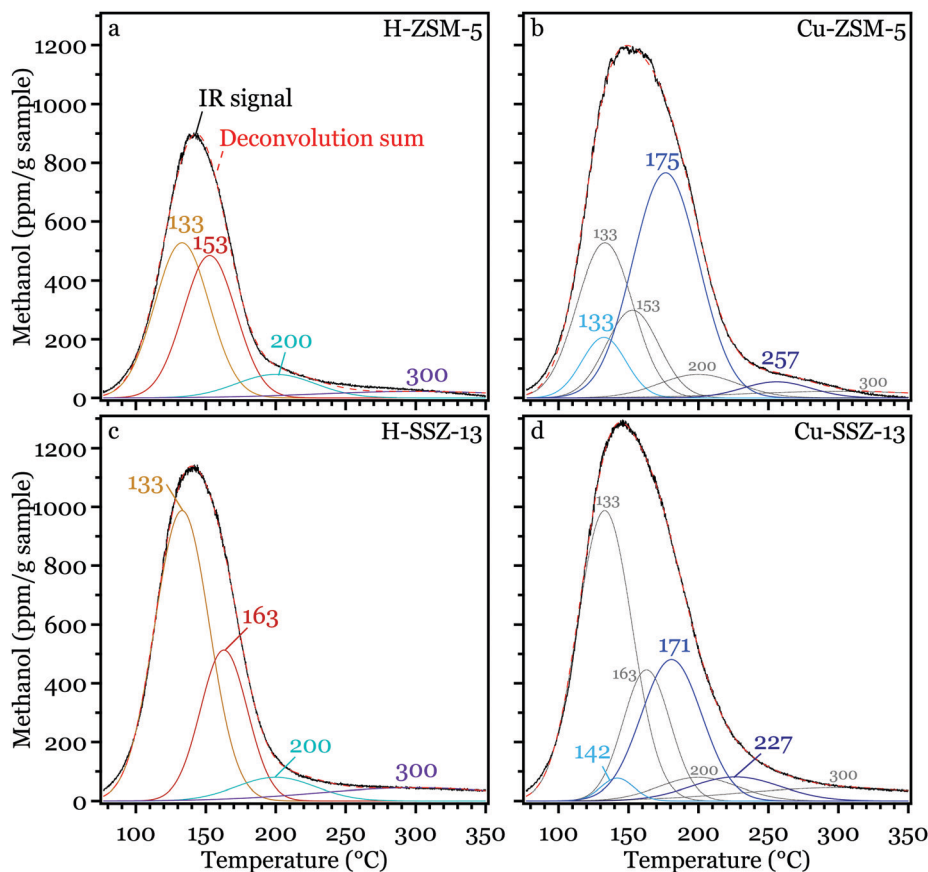*Phys. Chem. Chem. Phys.*, 2020, **22**, 6809–6817 | **6813**

Fig. 3 Deconvolution of methanol signals during methanol desorption from the pre-oxidized (a) H-ZSM-5, (b) Cu-ZSM-5, (c) H-SSZ-13 and (d) Cu-SSZ-13 samples. For the Cu-ZSM-5 and Cu-SSZ-13 samples, extra deconvoluted peaks (blue) were added based on the deconvolution of the H-ZSM-5 and H-SSZ-13 samples. The sum of the deconvoluted peaks is shown as red dashed lines and the center of the deconvoluted peaks is marked with numbers.

of Gaussian curves are used to achieve a reasonable fitting. The origin of these fitted functions is related to certain adsorption sites or desorption mechanisms which will be explained later in the Discussion section. Fig. 4 presents the theoretical methanol desorption profile from various Cu and zeolite sites in the Cu-ZSM-5 and Cu-SSZ-13 samples. Compared to the experiments, only the Brønsted acid site, the silanol site, and the Cu–OH–Cu desorb at relevant temperatures. The CuOCu, CuO, and CuOH sites bind methanol too weakly and desorb at too low temperatures, while the Cu monomer and Cu–Cu dimer binds methanol too strongly. From the calculations, one could be tempted to draw the conclusion that only the Cu–OH–Cu dimer is the relevant adsorption site with copper, since the bare copper species (Cu and Cu–Cu) bind too strongly and are relevant where DME and CO have formed at high temperatures. Although appealing, one should be careful about drawing such bold conclusions from these results since this is a relatively simple model only including desorption and adsorption. Furthermore, we performed a sensitivity analysis wherein we changed the binding energy of methanol ±0.1 eV (see ESI,† Fig. S9). This energy is much smaller than the uncertainty attributed to *e.g.* different exchange–correlation functionals.[53] This introduced change in binding energy shifts the desorption curves around ±35 °C. This demonstrates that there is some

uncertainty as to the exact position of the desorption peaks. Due to the higher Al content in Cu-SSZ-13, there are likely to be Cu monomers with two Al in the same six-membered ring, forming Cu^{II} species. This introduces a shift in methanol binding energies and can make these relevant in the temperature window for methanol formation, see Fig. S12 (ESI†). What we can see from the calculations is that there is a trend in bond strength and the bonding configuration between the different sites. The strongest methanol bond is to the bare Cu sites, both monomers and dimers, where methanol binds oxygen to the copper(s) forming a strong Cu–O bond or bonds. The second strongest methanol bond is to the OH sites where methanol binds oxygen forming a hydrogen bond situation with an intermediate water-like structure. This is the case as well for the Cu monomer and dimer as for the Brønsted and silanol sites. The weakest methanol bond is to the CuO sites where methanol binds hydrogen forming a hydrogen bond but without the intermediate water-like structure. This is sketched in Fig. 5.

As shown in Fig. 3a and c, for both the H-ZSM-5 and H-SSZ-13 samples, two peaks centered at 133 and 153–163 °C contribute largely to the methanol desorption profiles. The position of the peak centered at around 133 °C coincides with the methanol desorption profile of the SiO_2 sample (Fig. 1a). It is anticipated that the origin of this peak is mainly associated with methanol

6814 | *Phys. Chem. Chem. Phys.*, 2020, **22**, 6809–6817
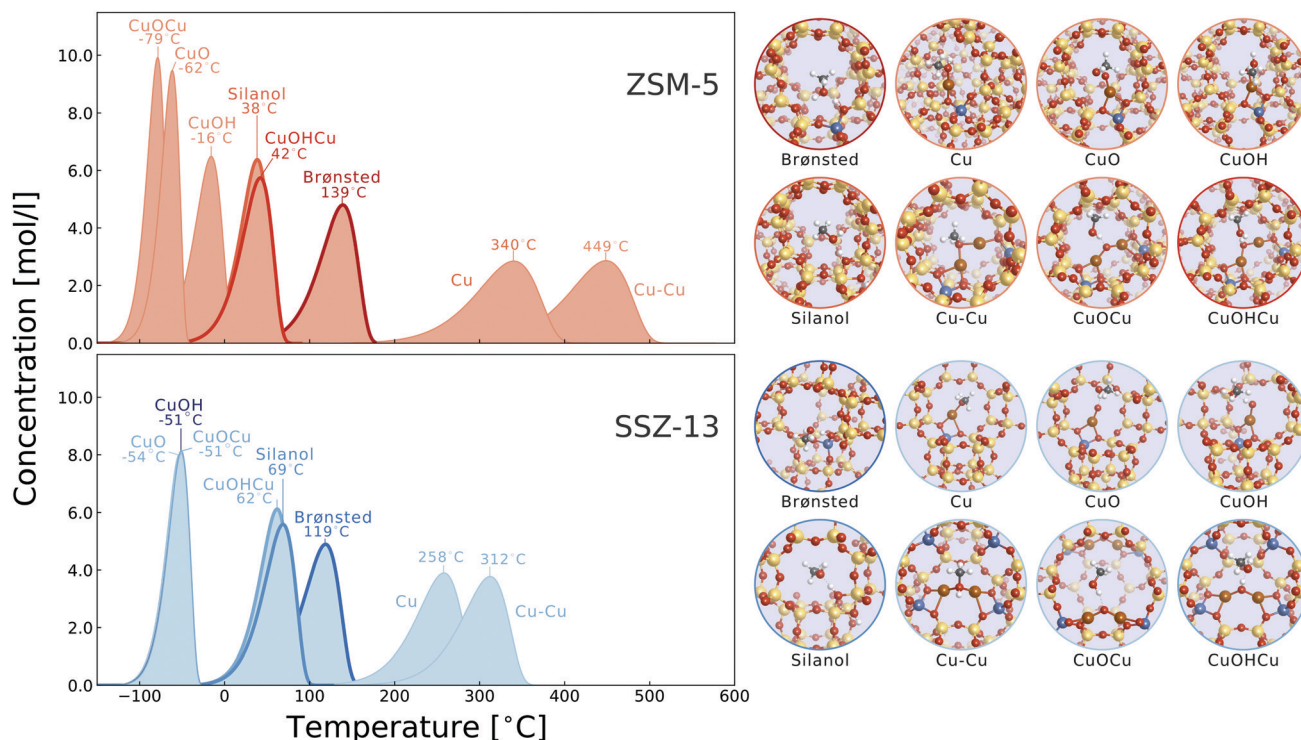
This journal is © the Owner Societies 2020

Fig. 4 Calculated desorption profiles from first-principles calculations for ZSM-5 in the top panel and SSZ-13 in the lower panel. The peak temperature is shown for each site and an illustration of the site is shown as insets to the right. The relevant curves are highlighted. Atomic colours: silicon: yellow, oxygen: red, aluminum: blue, copper: brown, hydrogen: white, and carbon: gray.
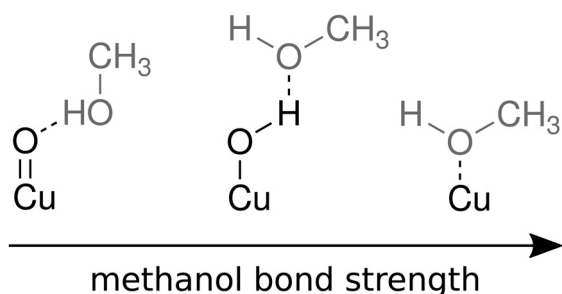

Fig. 5 Sketch of the methanol bonding to the different sites. The strongest bond to methanol is on the Cu sites, where methanol binds oxygen forming a strong Cu–O bond. The second to strongest bond is on the OH-sites (including the Brønsted and silanol sites) where methanol bonds with oxygen forming a hydrogen bond, also forming a water similar structure. Methanol binds the weakest to the CuO site where a hydrogen bond is formed to the methanol hydrogen.

desorption from the silanol groups in the zeolites. While for the peak centered at 153–163 °C, one possible explanation is that it is related to methanol desorption from the Brønsted acid sites in the zeolites. These anticipations are supported by the theoretical calculations shown in Fig. 4, where methanol desorbs at higher temperatures from the Brønsted acid sites than from the silanol groups. Additionally, minor contributions from methanol desorption at temperatures higher than 170 °C are evident for both the H-ZSM-5 and H-SSZ-13 samples. At temperatures higher than 170 °C, DME starts to form from pre-adsorbed methanol over the H-ZSM-5 and H-SSZ-13 samples

(as shown in Fig. 1b), indicating that methanol dissociates at such temperatures. Therefore, the two deconvoluted peaks at higher temperatures (centered above 200 °C) for the H-ZSM-5 and H-SSZ-13 samples are presumably associated with methanol adsorbed, dissociated, then recombined and desorbed from the zeolites.

For the Cu-ZSM-5 and Cu-SSZ-13 samples, contributions of methanol desorbed from the Cu sites are clearly indicated by the blue curves shown in Fig. 3b and d. It should be noted that the negative contribution from the Brønsted acid sites covered by Cu is taken into consideration here by reducing the amplitude of the Gaussian functions centred at 153 or 163 °C accordingly for the Cu-ZSM-5 and Cu-SSZ-13 samples, respectively. For both Cu-ZSM-5 and Cu-SSZ-13 samples, contributions of methanol desorption from the Cu sites at low temperatures (peak centered at 133 and 142 °C, respectively), medium temperatures (peak centered around 173 °C) and high temperatures (peak centered above 220 °C) are evident. Though it is clear that different Cu species are involved in methanol adsorption and desorption, the nature of these sites remains unclear. From the theoretical calculations, one may anticipate that hydrated Cu dimer species, i.e. Cu–OH–Cu, contribute largely to the low temperature peaks for both Cu-zeolite samples. Moreover, the formation of hydrated Cu species is likely due to the OH rich environment upon methanol adsorption. The largest contribution for the Cu-ZSM-5 and Cu-SSZ-13 samples, however, is the Gaussian curve centred around 173 °C. At such medium temperatures (170–230 °C), methanol and DME desorb simultaneously from

This journal is © the Owner Societies 2020

Phys. Chem. Chem. Phys., 2020, 22, 6809–6817 | 6815

the Cu-ZSM-5 and Cu-SSZ-13 samples. Moreover, methoxy species is evidently observed in the IR spectra of the Cu-ZSM-5 and Cu-SSZ-13 samples at 225 °C (Fig. 2b). Therefore, it is speculated that methanol dissociates over the Cu species at this temperature range, and the formed methoxy species is subsequently converted to either methanol or DME which desorbs from the Cu-zeolite samples. Similar to the high-temperature desorption peaks of the zeolite samples, the high-temperature peaks for the Cu-ZSM-5 and Cu-SSZ-13 samples are presumably associated with the desorption of dissociatively adsorbed methanol on the Cu sites.

4 Conclusions

This study shows that well-dispersed Cu ions/clusters in the zeolites interact strongly with methanol and its derivatives. Formation and desorption of DME are influenced by the ion-exchanged Cu as well as the zeolite framework structure. Effluent DME is observed at higher temperatures for zeolites functionalized with copper and the CHA framework structure shifts the DME desorption to higher temperatures compared to the MFI framework structure. Moreover, the introduction of Cu species increases the amount of CO formed and decreases its formation/desorption temperature.

Conflicts of interest

There are no conflicts to declare.

Acknowledgements

Notes and references

1 A. M. Beale, F. Gao, I. Lezcano-Gonzalez, C. H. F. Peden and J. Szanyi, *Chem. Soc. Rev.*, 2015, **44**, 7371–7405.

2 I. Yarulina, A. D. Chowdhury, F. Meirer, B. M. Weckhuysen and J. Gascon, *Nat. Catal.*, 2018, **1**, 398–411.

3 J. S. Woertink, P. J. Smeets, M. H. Groothaert, M. A. Vance, B. F. Sels, R. A. Schoonheydt and E. I. Solomon, *Proc. Natl. Acad. Sci. U. S. A.*, 2009, **106**, 18908–18913.

4 S. M. Campbell, X.-Z. Jiang and R. F. Howe, *Microporous Mesoporous Mater.*, 1999, **29**, 91–108.

5 R. Y. Brogaard, B. M. Weckhuysen and J. K. Nørskov, *J. Catal.*, 2013, **300**, 235–241.

6 U. Olsbye, S. Svelle, M. Bjørgen, P. Beato, T. V. W. Janssens, F. Joensen, S. Bordiga and K. P. Lillerud, *Angew. Chem., Int. Ed.*, 2012, **51**, 5810–5831.

7 M. A. C. Markovits, A. Jentys, M. Tromp, M. Sanchez-Sanchez and J. A. Lercher, *Top. Catal.*, 2016, **59**, 1554–1563.

8 R. Bulánek, B. Wichterlová, Z. Sobalík and J. Tichý, *Appl. Catal., B*, 2001, **31**, 13–25.

9 P. J. Smeets, M. H. Groothaert and R. A. Schoonheydt, *Catal. Today*, 2005, **110**, 303–309.

10 M. Ravi, M. Ranocchiari and J. A. van Bokhoven, *Angew. Chem., Int. Ed.*, 2017, **56**, 16464–16483.

11 M. H. Mahyuddin, Y. Shiota and K. Yoshizawa, *Catal. Sci. Technol.*, 2019, **9**, 1744–1768.

12 K. Narsimhan, V. K. Michaelis, G. Mathies, W. R. Gunther, R. G. Griffin and Y. Román-Leshkov, *J. Am. Chem. Soc.*, 2015, **137**, 1825–1832.

13 F. Gao, N. M. Washton, Y. Wang, M. Kollár, J. Szanyi and C. H. Peden, *J. Catal.*, 2015, **331**, 25–38.

14 V. L. Sushkevich and J. A. van Bokhoven, *Catal. Sci. Technol.*, 2018, **8**, 4141–4150.

15 K.-H. Steinberg, H. Bremer and P. Falke, *Z. Chem.*, 1974, **14**, 110–111.

16 V. Kanazirev and N. Borisova, *Zeolites*, 1982, **2**, 23–28.

17 V. Kazansky and E. Pidko, *Catal. Today*, 2005, **110**, 281–293.

18 G. Spoto, S. Bordiga, A. Zecchina, D. Cocina, E. Gribov, L. Regli, E. Groppo and C. Lamberti, *Catal. Today*, 2006, **113**, 65–80.

19 V. Bolis, A. Barbaglia, S. Bordiga, C. Lamberti and A. Zecchina, *J. Phys. Chem. B*, 2004, **108**, 9970–9983.

20 S. Ceckiewicz, *J. Colloid Interface Sci.*, 1982, **90**, 183–190.

21 B. Hunger, S. Matysik, M. Heuchel and W.-D. Einicke, *Langmuir*, 1997, **13**, 6249–6254.

22 X. Wang, A. A. Arvidsson, M. O. Cichocka, X. Zou, N. M. Martin, J. Nilsson, S. Carlson, J. Gustafson, M. Skoglundh, A. Hellman and P.-A. Carlsson, *J. Phys. Chem. C*, 2017, **121**, 27389–27398.

23 Y. Jiang, M. Hunger and W. Wang, *J. Am. Chem. Soc.*, 2006, **128**, 11679–11692.

24 X. Wu, S. Xu, W. Zhang, J. Huang, J. Li, B. Yu, Y. Wei and Z. Liu, *Angew. Chem., Int. Ed.*, 2017, **56**, 9039–9043.

25 C.-M. Wang, R. Y. Brogaard, B. M. Weckhuysen, J. K. Nørskov and F. Studt, *J. Phys. Chem. Lett.*, 2014, **5**, 1516–1521.

26 International Zeolite Association Webpage, http://europe.iza-structure.org.

27 P. N. Plessow and F. Studt, *ACS Catal.*, 2017, **7**, 7987–7994.

28 B. Ipek, M. J. Wulfers, H. Kim, F. Göltl, I. Hermans, J. P. Smith, K. S. Booksh, C. M. Brown and R. F. Lobo, *ACS Catal.*, 2017, **7**, 4291–4303.

29 D. K. Pappas, E. Borfecchia, M. Dyballa, I. A. Pankin, K. A. Lomachenko, A. Martini, M. Signorile, S. Teketel, B. Arstad, G. Berlier, C. Lamberti, S. Bordiga, U. Olsbye, K. P. Lillerud, S. Svelle and P. Beato, *J. Am. Chem. Soc.*, 2017, **139**, 14961–14975.

30 W. Gruenert, N. W. Hayes, R. W. Joyner, E. S. Shpiro, M. R. H. Siddiqui and G. N. Baeva, *J. Phys. Chem.*, 1994, **98**, 10832–10846.

6816 | *Phys. Chem. Chem. Phys.*, 2020, **22**, 6809–6817

This journal is © the Owner Societies 2020

31 F. Giordanino, P. N. R. Vennestrøm, L. F. Lundegaard, F. N. Stappen, S. Mossin, P. Beato, S. Bordiga and C. Lamberti, *Dalton Trans.*, 2013, **42**, 12741–12761.

32 F. Göltl, A. M. Love and I. Hermans, *J. Phys. Chem. C*, 2017, **121**, 6160–6169.

33 C. Paolucci, A. A. Parekh, I. Khurana, J. R. Di Iorio, H. Li, J. D. Albarracin Caballero, A. J. Shih, T. Anggara, W. N. Delgass, J. T. Miller, F. H. Ribeiro, R. Gounder and W. F. Schneider, *J. Am. Chem. Soc.*, 2016, **138**, 6028–6048.

34 X. Wang, N. M. Martin, J. Nilsson, S. Carlson, J. Gustafson, M. Skoglundh and P.-A. Carlsson, *Catalysts*, 2018, **8**, 545.

35 M. Männikkö, X. Wang, M. Skoglundh and H. Härelind, *Appl. Catal., B*, 2016, **180**, 291–300.

36 G. Kresse and J. Furthmüller, *Comput. Mater. Sci.*, 1996, **6**, 15–50.

37 G. Kresse and J. Furthmüller, *Phys. Rev. B: Condens. Matter Mater. Phys.*, 1996, **54**, 11169–11186.

38 J. P. Perdew, K. Burke and M. Ernzerhof, *Phys. Rev. Lett.*, 1996, **77**, 3865–3868.

39 S. Grimme, J. Antony, S. Ehrlich and H. Krieg, *J. Chem. Phys.*, 2010, **132**, 154104.

40 S. R. Bahn and K. W. Jacobsen, *Comput. Sci. Eng.*, 2002, **4**, 56–66.

41 M.-L. Tsai, R. G. Hadt, P. Vanelderen, B. F. Sels, R. A. Schoonheydt and E. I. Solomon, *J. Am. Chem. Soc.*, 2014, **136**, 3522–3529.

42 A. A. Arvidsson, V. P. Zhdanov, P.-A. Carlsson, H. Grönbeck and A. Hellman, *Catal. Sci. Technol.*, 2017, **7**, 1470–1477.

43 L. Chen, T. V. W. Janssens and H. Grönbeck, *Phys. Chem. Chem. Phys.*, 2019, **21**, 10923–10930.

44 U. Engedahl, H. Grönbeck and A. Hellman, *J. Phys. Chem. C*, 2019, **123**, 26145–26150.

45 M. Niwa, N. Katada, M. Sawa and Y. Murakami, *J. Phys. Chem.*, 1995, **99**, 8812–8816.

46 L. Chen, T. V. W. Janssens, M. Skoglundh and H. Grönbeck, *Top. Catal.*, 2018, **62**, 93–99.

47 A. G. Pelmenschikov, G. Morosi, A. Gamba, A. Zecchina, S. Bordiga and E. A. Paukshtis, *J. Phys. Chem.*, 1993, **97**, 11979–11986.

48 P. J. Smeets, J. S. Woertink, B. F. Sels, E. I. Solomon and R. A. Schoonheydt, *Inorg. Chem.*, 2010, **49**, 3573–3583.

49 M. C. Kung, S. S. Y. Lin and H. H. Kung, *Top. Catal.*, 2012, **55**, 108–115.

50 T. Nobukawa, M. Yoshida, S. Kameoka, S.-I. Ito, K. Tomishige and K. Kunimori, *J. Phys. Chem. B*, 2004, **108**, 4071–4079.

51 B. R. Wood, J. A. Reimer, A. T. Bell, M. T. Janicke and K. C. Ott, *J. Catal.*, 2004, **225**, 300–306.

52 K. I. Hadjiivanov, M. M. Kantcheva and D. G. Klissurski, *J. Chem. Soc., Faraday Trans.*, 1996, **92**, 4595–4600.

53 J. Wellendorff, K. T. Lundgaard, A. Møgelhøj, V. Petzold, D. D. Landis, J. K. Nørskov, T. Bligaard and K. W. Jacobsen, *Phys. Rev. B: Condens. Matter Mater. Phys.*, 2012, **85**, 235149.

This journal is © the Owner Societies 2020

Phys. Chem. Chem. Phys., 2020, **22**, 6809–6817 | **6817**